Supplement of Solid Earth, 16, 1289–1306, 2025
https://doi.org/10.5194/se-16-1289-2025-supplement

Solid Earth
Open Access

Supplement of

Deformation and exhumation in thick continental crusts induced by valley incision of elevated plateaux

Thomas Geffroy et al.

Correspondence to: Philippe Yamato (philippe.yamato@univ-rennes.fr)

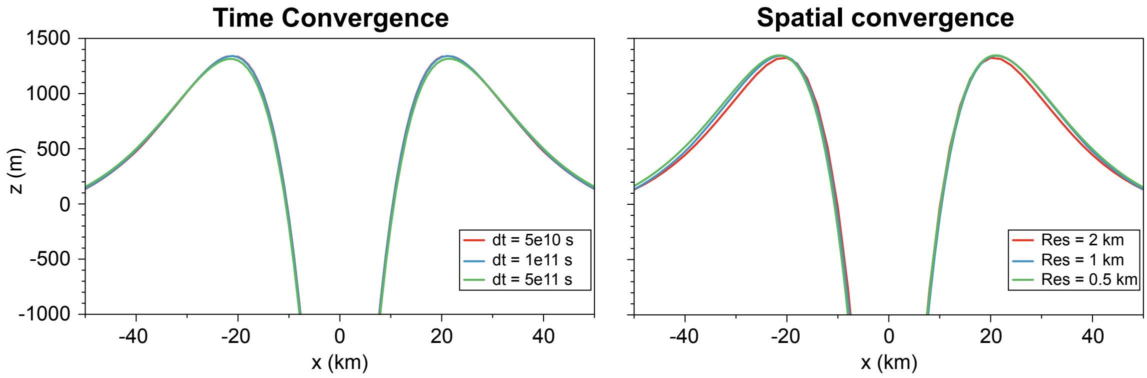

Figure S1: Convergence test. Topography of the model after 1.6 Myr for (left) different time steps (dt) and (right) different mesh-grid resolution (Res).

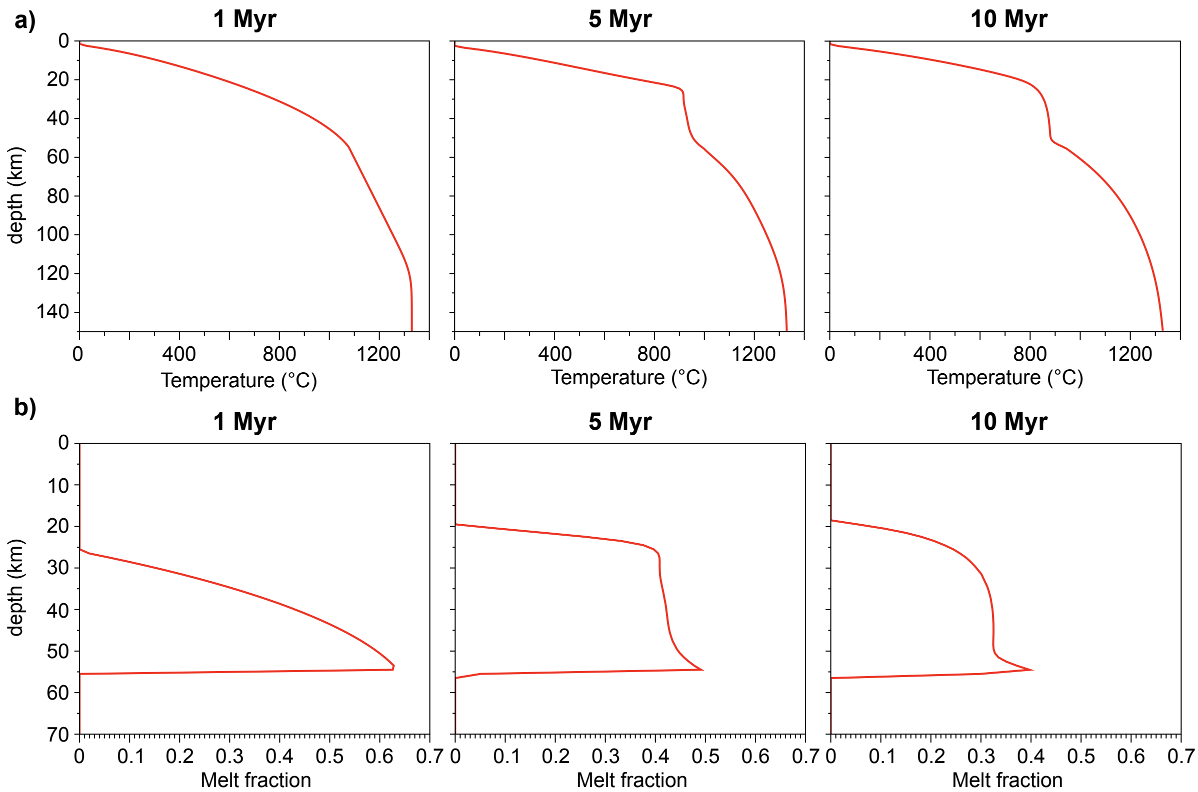

Figure S2: Vertical profiles at the center of the valley for the reference model at different time of (a) the temperature and (b) the melt fraction of the crust.

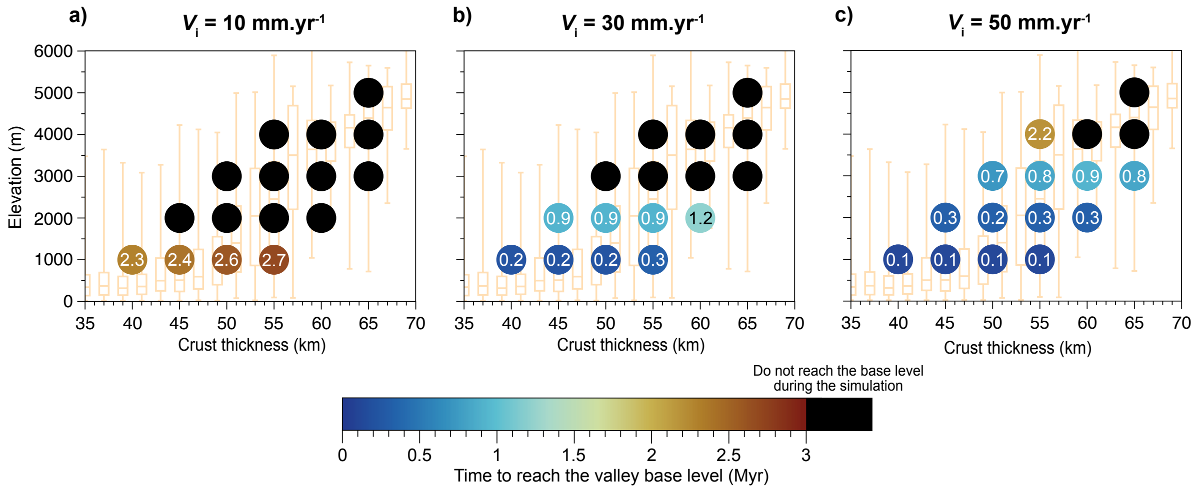

Figure S3: Time for the valley to reach the base level for a) V_i = 10 mm.yr^{-1}, b) V_i = 30 mm.yr^{-1} , and c) V_i = 50 mm.yr^{-1}. Values presented inside the circles are in Myr. Black points represent models in which the valley do not reach the base level in the simulation timeframe (i.e., 10Myr).

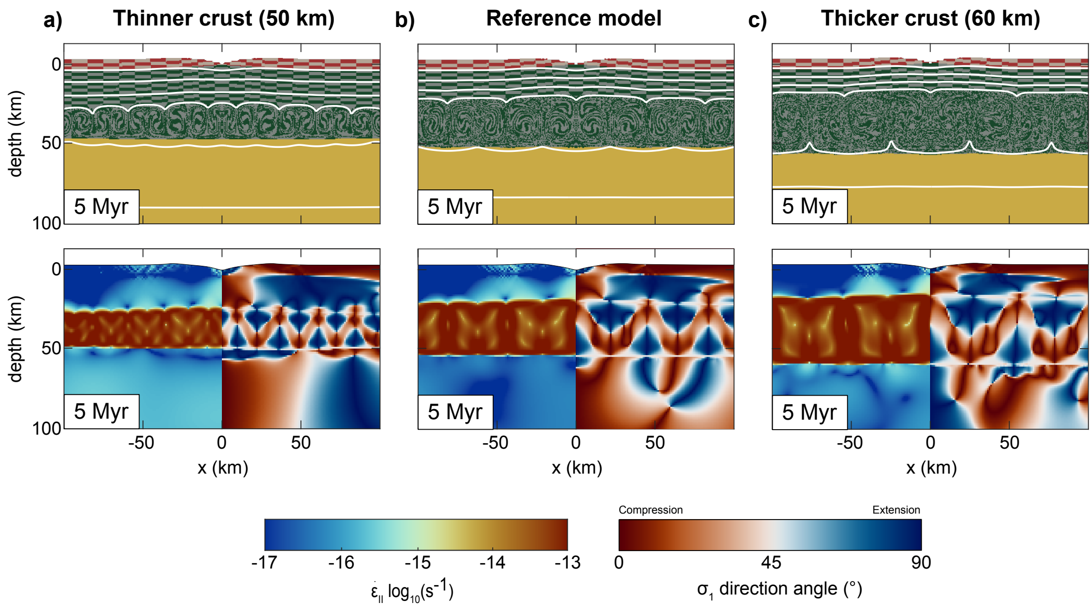

Figure S4: Models snapshots after 5 Myr for (a) a thin crust model (50 km), (b) the reference model (55km), and (c) a thick crust model (60 km). First line represents the material and thermal evolution. White lines represents each 200°C isotherm. Second line represents the second invariant of the strain rate (left) and the evolution of the σ_1 direction angle (right).

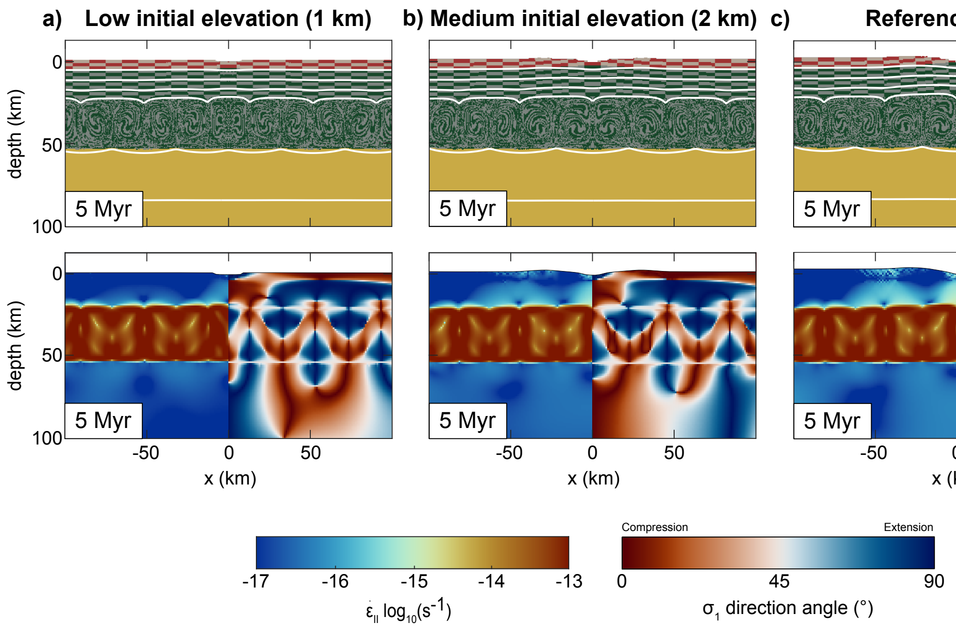

Figure S5: Models snapshots after 5 Myr for (a) low initial plateau elevation model (1 km), (b) a medium initial plateau elevation model (2 km), and (c) the reference model (3 km). First line represents the material and thermal evolution. White lines represent each 200°C isotherm. Second line represents the second invariant of the strain rate (left) and the evolution of the σ_1 direction angle (right).

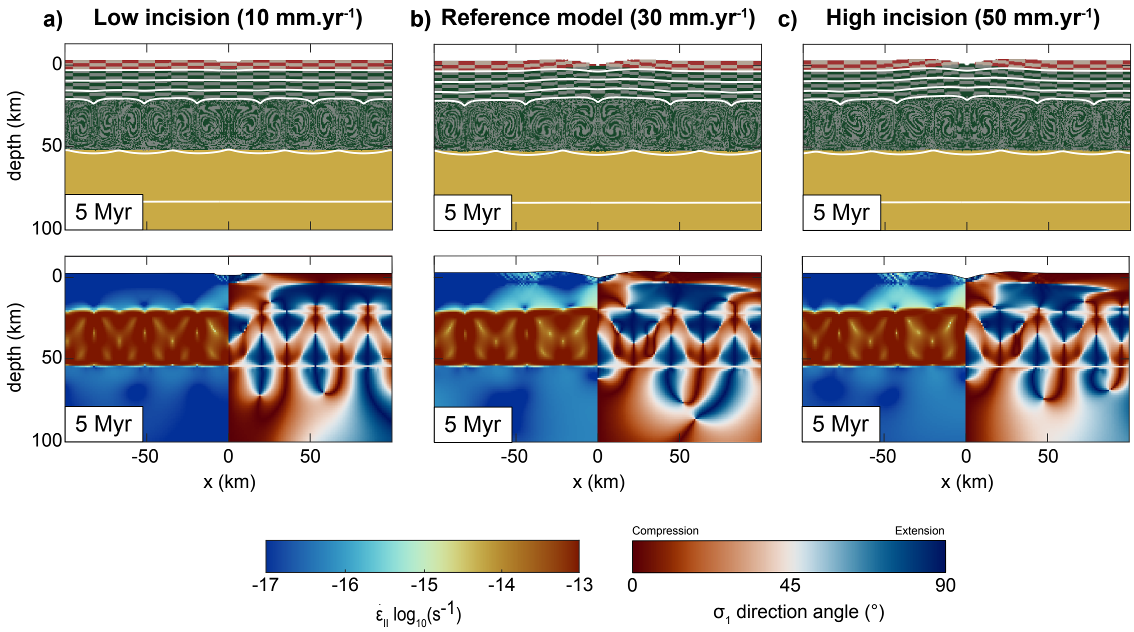

Figure S6: Models snapshots after 5 Myr for (a) low incision velocity model (10 mm.yr^{-1}), (b) the reference model (30 mm.yr^{-1}), and (c) a high incision velocity model (50 mm.yr^{-1}). First line represents the material and thermal evolution. White lines represent each 200°C isotherm. Second line represents the second invariant of the strain rate (left) and the evolution of the σ_1 direction angle (right).

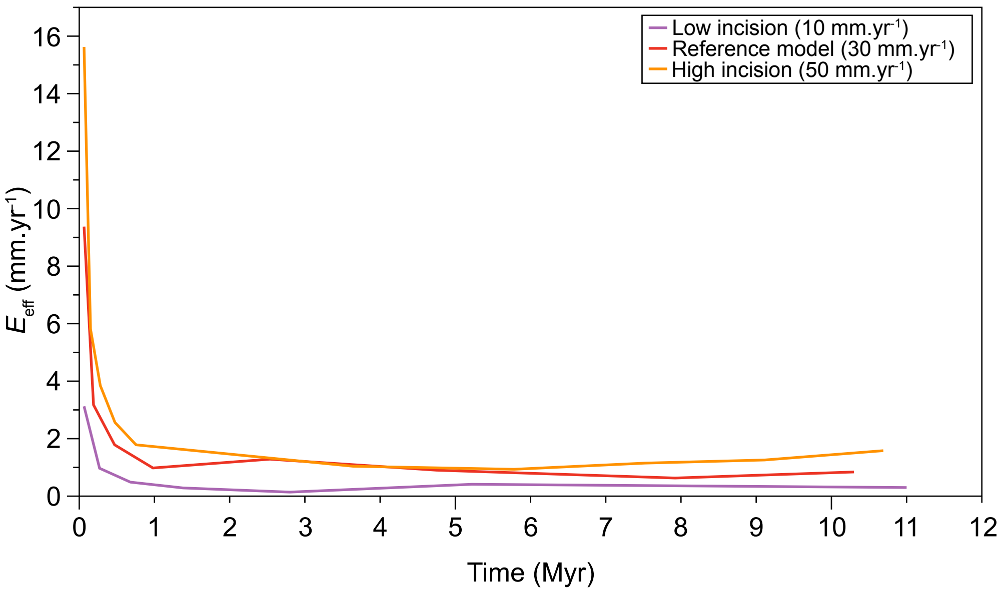

Figure S7: Time evolution of the effective erosion at the center of the valley (E_{eff}) for the low incision model (10 mm.yr^{-1}), the reference model 30 mm.yr^{-1}), and the high incision model (50 mm.yr^{-1}). All these models are performed with a initial plateau elevation of 3 km, and a crustal thickness of 55 km.

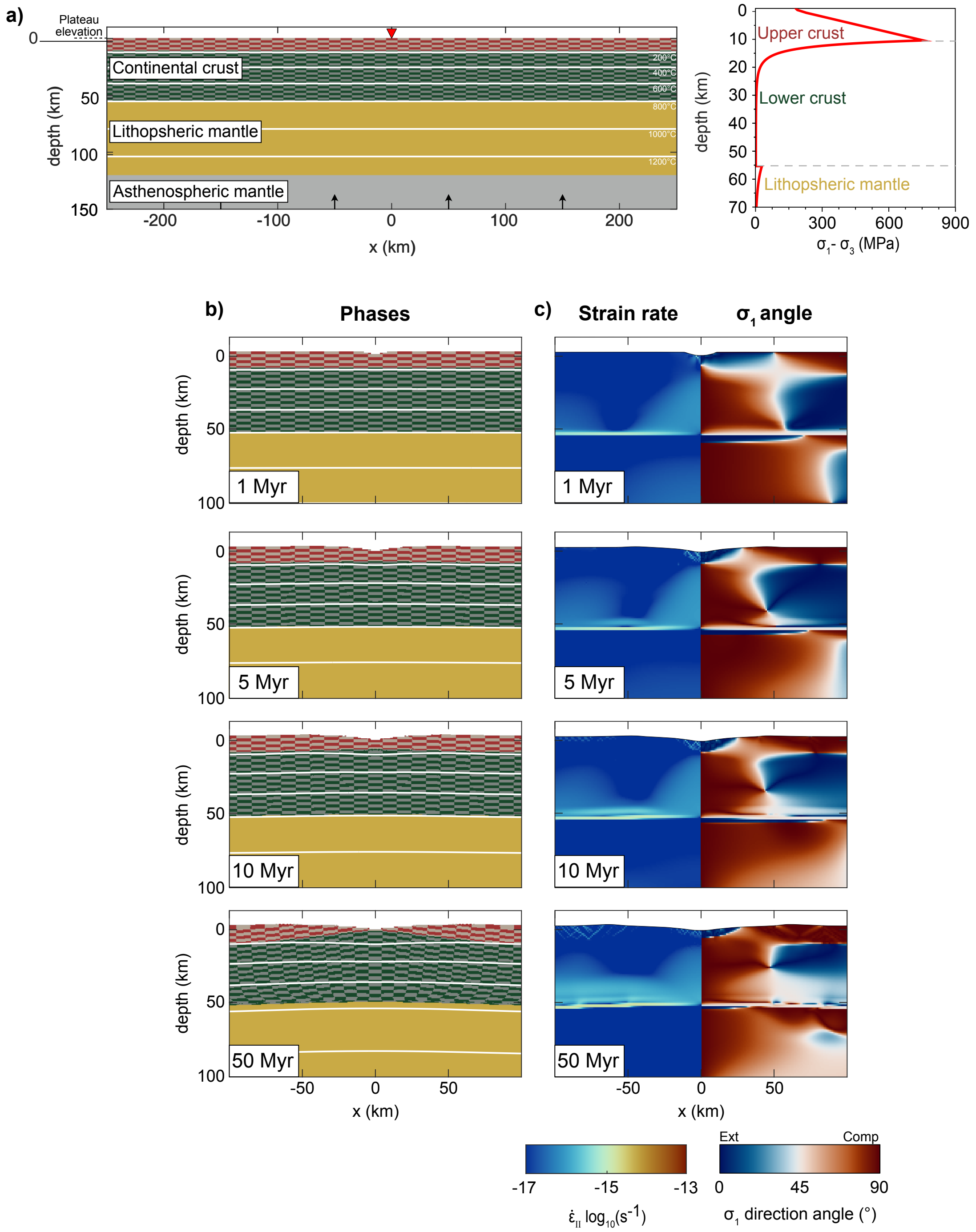

Figure S8: a) Initial model setup for the reference model with a reduced radiogenic heat production of 1.5 ×10^{-7} W.m^{2}, and associated yield strength profile from the surface to 70 km depth (see Figure 2 for details). Time evolution of the model after 1, 5, 10 and 50 Myr. (b) material and thermal evolution. White lines represent each 200°C isotherm. Color legend is as for Figure 2b. (b) left: Evolution of the second invariant of the strain rate. right: Evolution of the angle between the maximum principal stress (σ_1) and the vertical axis).

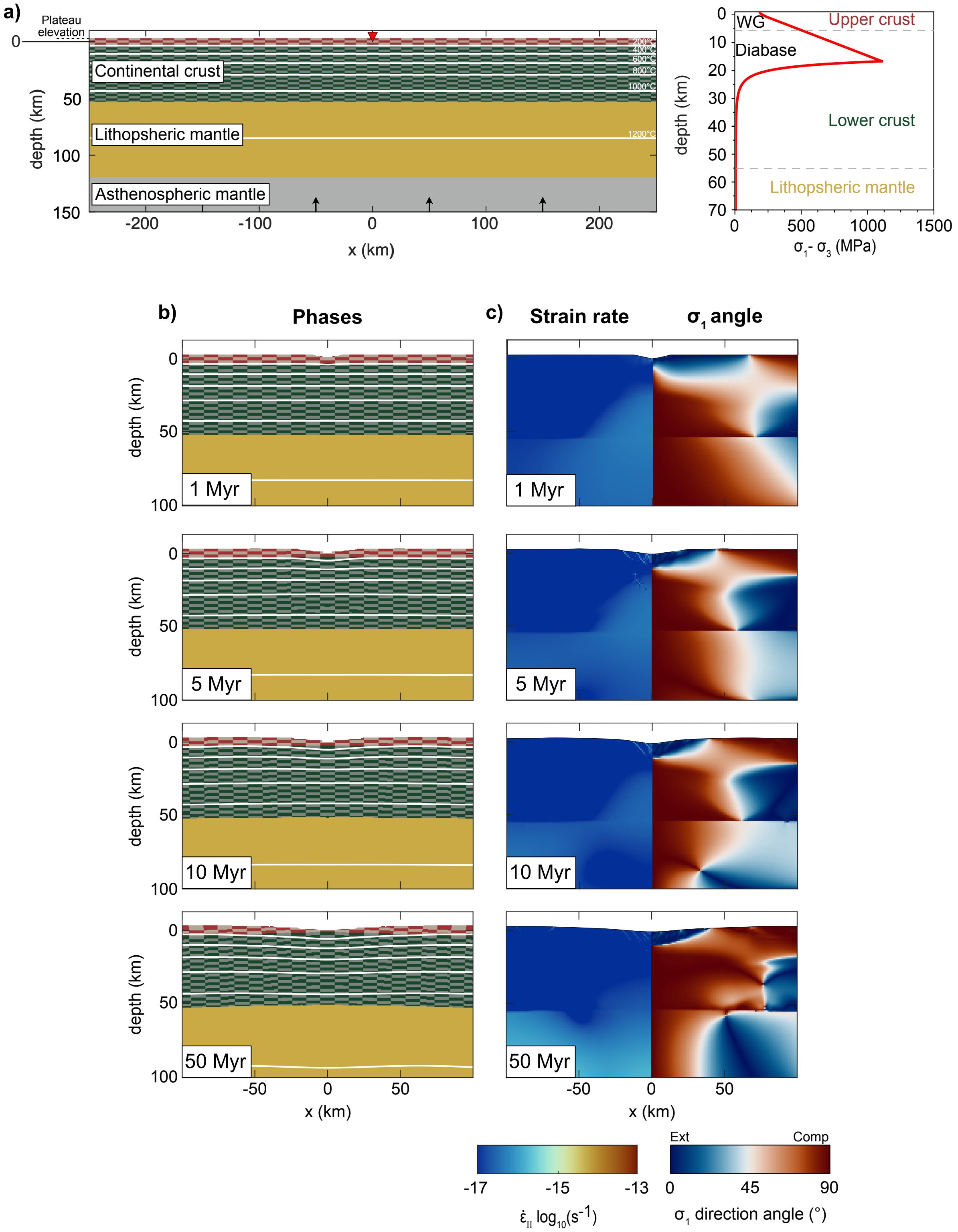

Figure S9: a) Initial model setup for the reference model with a Maryland Diabase lower crust (*n* = 4.7; *A* = 5.0477×10^{-28} Pa^{-n}.s^{-1}; *Q* = 485×10^{3} J.mol^{-1}) (Mackwell et al., 1998) and associated yield strength profile from the surface to 70 km depth (see Figure 2 for details) (WG = Westerly Granite). Time evolution of the model after 1, 5, 10 and 50 Myr. (b) material and thermal evolution. White lines represent each 200°C isotherm. Color legend is as for Figure 2b. (b) left: Evolution of the second invariant of the strain rate. right: Evolution of the angle between the maximum principal stress (σ_1) and the vertical axis).

Model name	Crustal thickness (H) (km)	Initial plateau elevation (h_P) (km)	Incision velocity (V_i) ($mm.yr^{-1}$)
40-1_Vi10	40	1	10
40-1_Vi30	40	1	30
40-1_Vi50	40	1	50
45-1_Vi10	45	1	10
45-1_Vi30	45	1	30
45-1_Vi50	45	1	50
45-2_Vi10	45	2	10
45-2_Vi30	45	2	30
45-1_Vi50	45	2	50
50-1_Vi10	50	1	10
50-1_Vi30	50	1	30
50-1_Vi50	50	1	50
50-2_Vi10	50	2	10
50-2_Vi30	50	2	30
50-2_Vi50	50	2	50
50-3_Vi10	50	3	10
50-3_Vi30	50	3	30
50-3_Vi50	50	3	50
55-1_Vi10	55	1	10
55-1_Vi30	55	1	30
55-1_Vi50	55	1	50
55-2_Vi10	55	2	10
55-2_Vi30	55	2	30
55-2_Vi50	55	2	50
55-3_Vi10	55	3	10
55-3_Vi30	55	3	30
55-3_Vi50	55	3	50
55-4_Vi10	55	4	10
55-4_Vi30	55	4	30
55-4_Vi50	55	4	50
60-2_Vi10	60	2	10
60-2_Vi30	60	2	30
60-2_Vi50	60	2	50
60-3_Vi10	60	3	10
60-3_Vi30	60	3	30
60-3_Vi50	60	3	50
60-4_Vi10	60	4	10
60-4_Vi30	60	4	30
60-4_Vi50	60	4	50
65-3_Vi10	65	3	10
65-3_Vi30	65	3	30
65-3_Vi50	65	3	50
65-4_Vi10	65	4	10
65-4_Vi30	65	4	30
65-4_Vi50	65	4	50
65-5_Vi10	65	5	10
65-5_Vi30	65	5	30
65-5_Vi50	65	5	50

Table S1: Models name and parameters used in the parametric study.

References

Mackwell, S. J., Zimmerman, M. E., & Kohlstedt, D. L. (1998). High-temperature deformation of dry diabase with application to tectonics on Venus. *Journal of Geophysical Research: Solid Earth*, *103*(B1), 975-984. https://doi.org/10.1029/97JB02671